

Loop current states and their stability in small fractal lattices of Bose-Einstein condensates

Georg Koch¹ and Anna Posazhennikova¹

¹*Institut für Physik, Universität Greifswald, 17487 Greifswald, Germany*

(Dated: January 17, 2024)

We consider a model of interacting Bose-Einstein condensates on small Sierpinski gaskets. We study eigenstates which are characterised by cyclic supercurrents per each triangular plaquette ("loop" states). For noninteracting systems we find at least three classes of loop eigenmodes: standard; chaotic and periodic. Standard modes are those inherited from the basic three-site ring of condensates with phase differences locked to $2\pi/3$. Standard modes become unstable in the interacting system but only when interaction exceeds a certain critical value u_c . Chaotic modes are characterised by very different circular currents per plaquette, so that the usual symmetry of loop currents is broken. Circular supercurrents associated with chaotic modes become chaotic for any finite interaction, signalling the loss of coherence between the condensates. Periodic modes are described by alternating populations and two different phase differences. The modes are self-similar and are present in all generations of Sierpinski gasket. When interaction is included, circular current of such a mode becomes periodic in time with the amplitude growing linearly with interaction. Above a critical interaction the amplitude saturates signalling a transition to a macroscopic self-trapping state originally known from a usual Bose Josephson junction. We perform a systematic analysis of this novel and rich physics.

I. INTRODUCTION

Fractal lattices are structures of non-integer dimension which are characterised by scale invariance rather than translational invariance of a typical Euclidean lattice²². In the context of solid state physics Sierpinski gasket lattices are particularly popular because their statistical mechanical properties and transport can be calculated analytically¹⁵. Their one-particle spectrum and density of states can be found by a relatively simple decimation procedure, resulting in discrete mostly degenerate eigenenergies with underlying fractal properties^{7,34}. Corresponding eigenstates are also nontrivial, with many of them being localized just due to the gasket geometry, i.e. in the absence of any disorder.

Recently, a number of experimental successes in realisation of fractal structures^{3,12,17,20,36,48} have been achieved. This has revived the interest towards fractals, in particular, within theoretical condensed-matter community with latest publications covering a broad range of topics, including electron transport^{42,43,45}, localisation^{23,28}, topology^{4,14,24,27}, flat bands²⁹ and quantum phase transitions^{19,47}, to mention a few.

In this work we consider a system of weakly-linked interacting Bose-Einstein condensates (BECs) placed on a small fractal lattice, which is in essence a mean-field description of Bose-Hubbard model on the lattice. The advantage of using BECs is their high tunability and unprecedented quantum state control (see for instance⁹ and references therein). Since we study small systems, our goal is not only to understand the system at hand, but also to answer the old but still important question whether one can infer information on physics of larger systems from study of their finite-sized counterparts. We show, that this is indeed possible to some degree for given systems.

If two BECs are weakly linked, there is an oscillating current between them due to the Josephson effect³⁷. When three condensates are joined in a ring, then Josephson effect gives rise to a cyclic supercurrent along the ring, provided phase differences between neighboring sites are fixed to $2\pi/3$ and all populations are the same^{30,41}. An N_s -site ring would need the phase differences equal to $2\pi/N_s$ in order to maintain a cyclic supercurrent. Such cyclic currents are interesting per se since they represent topological defects (vortices) and are relevant for Kibble-Zurek scenario and quantum phase transitions^{10,30,41}. Rings of condensates supporting stable circular flows were recently realised experimentally with polariton condensates⁵.

When small rings of condensates are arranged into a regular lattice, one would expect under certain conditions circular currents per plaquette, exemplifying loop current lattice states. Loop current states are quite popular in strongly-correlated electron systems where they are related to orbital magnetism and are signatures of exotic states of matter, e.g. exotic superconductivity^{16,25,44}. In lattices of neutral bosonic systems synthetic magnetic fields were realised giving rise to circular plaquette currents corresponding to fluxes with tunable values^{1,26}.

In our work we consider a simpler case of a lattice with deep potential wells accomodating mini BECs with imprinted phases. The fact that the lattice has a fractal geometry makes the problem non trivial, since it is not a priori clear whether such a formation would support circular plaquette currents due to a complicated discrete structure of the single-particle spectrum. Another question is, when it does, whether those currents remain stable in an interacting system. In the following we aim to answer these questions in detail.

With the help of a decimation procedure developed previously by the authors of Refs.^{7,34} we show that loop

states can indeed be realized in Sierpinski gaskets of BECs, and in several different ways. For clarity, we divide them into three classes, all associated with various excited states. The ground state can only be described by equal site populations and zero phase differences between all sites and is therefore not looped.

The three classes differ not only in realization of loop modes, but also in the way the looped states dynamics changes in the presence of interaction. For example, *standard* modes are in many ways similar to the aforementioned modes of three-site condensate rings. Specifically, there is a critical interaction u_c at which the corresponding fixed point in the phase space changes from stable to unstable. The circular current stays the same after interaction is turned on, but for $u > u_c$ becomes chaotic upon a tiny perturbation. Interestingly, the critical interaction u_c is different in each generation and is decreasing with the size of fractal increasing.

The other class of loop eigenstates is termed by us *chaotic*. Chaotic eigenmodes are characterised by broadly distributed phase differences as well as population differences. All plaquettes have different circular currents, so that the usual symmetry of loop currents is broken. These modes do not survive in an interacting system, because any circular current associated with such a mode immediately acquires chaotic dynamics.

Another class of modes, which we refer to as *periodic*, comprises states deep inside the largest gap of the spectrum. On the contrary to chaotic modes, periodic states are represented by only two phase differences and only two population differences at any stage. As a result the phase portrait of the multidimensional noninteracting fixed point has effectively only two subspaces: stable and unstable. This fixed point changes when the interaction is on, but the fundamental structure of the phase portrait remains the same.

When interacting system is initially at the noninteracting fixed point, circular currents begin to oscillate in time. The character of these oscillations depends on the interaction. For sufficiently small interaction the amplitudes of the oscillations grow linearly with time. When interaction exceeds a certain value u_{ST} , the amplitude saturates. The interaction u_{ST} marks thus a transition of the system to a macroscopically self-trapped state similar to the one well-known from the usual bosonic Josephson junctions³⁷.

We also find loop states at the gap edge, which have another unusual property- they only have supercurrents along their inner edges, effectively dividing the system into two independent subsystems. With increasing generation these modes start resembling chaotic ones, although the initial decoupling remains in place.

The paper is organized as follows: in Section II we briefly discuss the model and equations of motion. In Section III we consider noninteracting fractals and their loop eigenstates. For convenience of the reader we divide this Section into three subsections: the first subsection briefly outlines known results of an infinite Sierpinski gas-

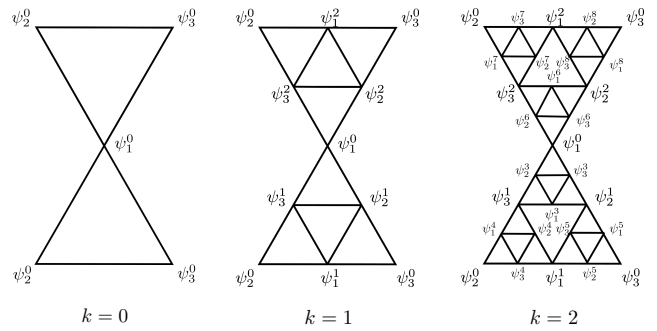


FIG. 1: First three stages of the Sierpinski gasket fractal. The wave functions on different nodes are denoted by an upper index representing the sub-triangle they belong to and a lower index which differentiates between sites within the sub-triangle. On the left the first stage of the mirrored gasket can be seen, since the mirrored sites are set to be equal they have the same upper index. In the middle stage two sub-triangles have been added, for the third stage on the right another six have been inserted. The sites denoted by the same wave-functions are the same sites. This is a result of juxtaposition of the two largest triangles in order to secure periodic boundary conditions.

ket, the second details loop eigenmodes of stages $k = 0$ and $k = 1$, whereas the last Subsection deals with all the loop modes of stage $k = 2$. Many analytical details are moved to Appendix B. In Section IV we scrutinise the dynamics of the found eigenstates once the interaction between bosons in condensates is taken into account. We subdivide this Section into three subsections depending on the class of loop modes, since they exhibit very different dynamics. We conclude in Section V.

II. MODEL AND EQUATIONS OF MOTION

We consider a system of N interacting bosons which are trapped in a fractal-shaped potential with the number of sites N_k depending on the generation k (specifically, we consider the first three generations of the Sierpinski gasket shown in Fig. 1). Generally bosons on a lattice are described by Bose-Hubbard hamiltonian¹³. For weak on-site interaction between bosons U and macroscopic site occupancies $\rho = N/N_k$ a mean-field approximation can be justified^{8,11,35,40}. The system is then described semi-classically by a condensate wave-function $\Psi = (\Psi_1, \Psi_2, \dots, \Psi_{N_k})$, where Ψ_i -s obey the discrete nonlinear Schrödinger equations

$$i\hbar \frac{\partial}{\partial t} \Psi_i(t) = U |\Psi_i(t)|^2 \Psi_i(t) - K \sum_{\langle j \rangle} \Psi_j(t) \quad (1)$$

where K describes tunneling between nearest neighbors. This is equivalent to Gross-Pitaevskii equations with spatial dependencies integrated out, which works surprisingly good even for a two-well potential².

Note that in description of equations we use a one-index site notations for simplicity, where possible. The sum in (1) goes over four nearest neighbours of site i . Condensate wave-functions are time-dependent complex functions

$$\Psi_i(t) = \sqrt{N_i(t)} e^{i\theta_i(t)}, \quad (2)$$

where N_i is the number of particles in the condensate on site i , θ_i is the local phase. Since the system under consideration is closed, the total particle number $N = \sum_i N_i(t)$ is conserved. It is convenient to normalise the wave -functions (2) by the root of the filling factor ρ as following

$$\psi_i = \frac{\Psi_i}{\sqrt{\rho}} = \sqrt{n_i(t)} e^{i\theta_i(t)}. \quad (3)$$

In this case $\sum_i n_i = N_k$.

Assuming $\hbar \equiv 1$ and introducing dimensionless interaction constant

$$u = \frac{U\rho}{K} \quad (4)$$

we get from (1) the final system of DNLS equations

$$i \frac{\partial}{\partial t} \psi_i(t) = u |\psi_i(t)|^2 \psi_i(t) - \sum_{\langle j \rangle} \psi_j(t). \quad (5)$$

We utilise periodic boundary conditions, employed in⁷ in order to calculate the spectrum of one-particle Schrödinger equation on such lattices. The boundary conditions utilise a mirrored gasket obtained by the juxtaposition of two identical generation k gaskets at their corresponding external sites. In this way each site has exactly four neighboring sites.

Instead of complex equations (5) one can also solve a set of real equations for conjugated variables n_i and θ_i

$$\begin{aligned} \dot{n}_i &= -2 \sum_{\langle j \rangle} \sqrt{n_i n_j} \sin(\theta_j - \theta_i), \\ \dot{\theta}_i &= -u n_i + \sum_{\langle j \rangle} \sqrt{\frac{n_j}{n_i}} \cos(\theta_j - \theta_i). \end{aligned} \quad (6)$$

We numerically evaluate the following quantities: pairwise phase differences between condensates on neighboring sites, pairwise population imbalances between condensates on neighboring sites and circular currents. We first define Josephson supercurrent between two adjacent condensates in the standard way

$$I_{i,i+1}^{m,l} = 2 \cdot \text{Im}(\psi_i^{m*} \psi_{i+1}^l). \quad (7)$$

Here we had to revert to our double-indexed notations explained in Fig. 1, for clarity. Circular current per chosen subsystem is defined as a sum over the Josephson sub-currents over all the structure divided by their number N_I

$$I = \frac{1}{N_I} \sum_{i=1}^{N_I} \sum_{m,l} I_{i,i+1}^{m,l}. \quad (8)$$

Generally we consider only the total circular current of the lower half fractal (summed over all the nodes). When the system under consideration is in one of its eigenstates, then this circular current is constant, as well as all the phase differences and population imbalances. We derive eigenstates analytically in Section III and verify numerically that circular currents remain indeed constant with time.

This time-independent behaviour changes, however, if we add non-zero u in our analysis, while using the eigenmodes as initial conditions. The resulting dynamics can be evaluated only numerically and reveals very different behavior depending on the initial conditions, i.e. on eigenstate classes. The detailed study of interacting systems is presented in Section IV.

III. LOOP CURRENT STATES OF THE NONINTERACTING SYSTEM

A. Loop eigenmodes of $k = 0$ and $k = 1$ stages

In this Section we derive eigenmodes of the noninteracting system for stages $k = 0$ and $k = 1$, which are characterised by loop currents. Eigenvalues for any stage are well-known and were derived by a decimation procedure in Refs.^{7,34} (see also a brief reminder in Appendix A). Note that periodic boundary conditions (see Fig. 1) were crucial for development of the decimation procedure and are therefore employed in our work as well.

The decimation procedure implies that some eigenvalues are derived from the others, and since this information is important for our derivations, Fig. 2 demonstrates a flowchart where we present all eigenvalues of the first three generations and relations between them. We also mark eigenvalues whose eigenstates we are not going to analyse since they can not maintain loop currents.

For stage $k = 0$ the Hamiltonian (expressed in the units of the coupling constant K) is trivial

$$\mathcal{H}_{k=0} = \begin{pmatrix} 0 & -2 & -2 \\ -2 & 0 & -2 \\ -2 & -2 & 0 \end{pmatrix}, \quad (9)$$

with eigenvalues $\epsilon_{k=0} \in \{-4, 2, 2\}$. The eigenmodes $|\Psi_{k=0}(\epsilon_{k=0})\rangle$ are also readily found

$$|\Psi_{k=0}(-4)\rangle = \begin{pmatrix} 1 \\ 1 \\ 1 \end{pmatrix}, \quad (10)$$

$$|\Psi_{k=0}(2)\rangle_{\pm} = \begin{pmatrix} 1 \\ e^{\pm i2\pi/3} \\ e^{\pm i4\pi/3} \end{pmatrix}. \quad (11)$$

where the loop eigenmodes correspond to the doubly degenerate level $\epsilon_{k=0} = 2$. These kind of states are well known from rings of condensates studies^{30,41,46}. State $|\Psi_{k=0}(-4)\rangle$ corresponds to the ground state and is the

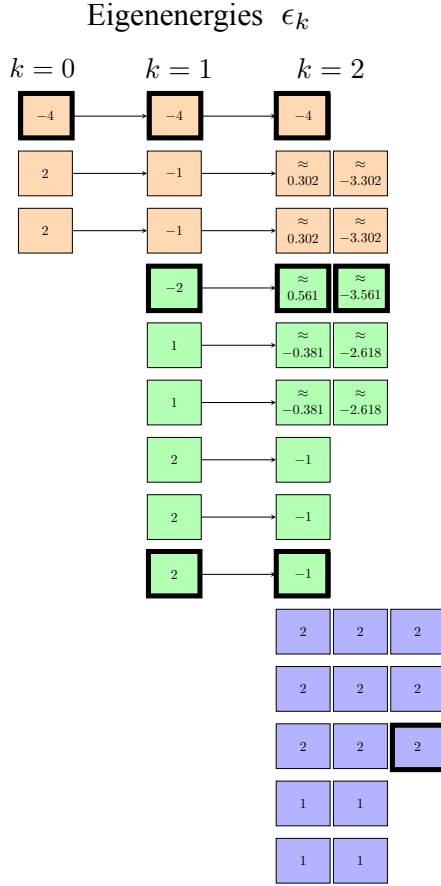


FIG. 2: Flowchart of all eigenenergies (in the units of K) for the first three generations of Sierpinski gasket. Values which have been generated by the recursion procedure (22) are connected by arrows with their ancestors. Those that are added on at a given stage without having direct predecessors are colored differently (e.g. the green values for $k=1$). Thick black frames mark eigenvalues whose eigenvectors will not have any loop currents, hence such states will not be considered in this work.

same in all generations of Sierpinski gasket (with the size increasing correspondingly).

Since we will use one of the loop eigenvectors for the derivation of loop states on stages $k=1$ and $k=2$, we introduce a short notation

$$V \equiv |\Psi_{k=0}(2)\rangle_+ . \quad (12)$$

At the next stage $k=1$ the system Hamiltonian still has a rather simple structure

$$\mathcal{H}_{k=1} = \begin{pmatrix} \hat{0} & \hat{S} & \hat{S} \\ \hat{S} & \hat{S} & \hat{0} \\ \hat{S} & \hat{0} & \hat{S} \end{pmatrix}, \quad \hat{S} = \begin{pmatrix} 0 & -1 & -1 \\ -1 & 0 & -1 \\ -1 & -1 & 0 \end{pmatrix} \quad (13)$$

with eigenvalues $\epsilon_{k=1} \in \{-4, 2, 2, 2, -1, -1, -2, 1, 1\}$. Since we are only interested in loop eigensates, and they always come in conjugated pairs, we explore states corresponding to the degenerate eigenvalues $\{2, \pm 1\}$.

Now we notice that V is an eigenstate of \hat{S} with eigenvalue $\lambda_s = 1$. We can use this fact for finding loop eigenmodes of the Hamiltonian $\mathcal{H}_{k=1}$. We notice that the simplest 3×3 anticirculant matrix representing the structure of the Hamiltonian reads

$$\begin{pmatrix} 0 & 1 & 1 \\ 1 & 1 & 0 \\ 1 & 0 & 1 \end{pmatrix}, \quad (14)$$

and eigenvectors of this matrix are readily found: $(1, 1, 1)^T$, $(-2, 1, 1)^T$ and $(0, -1, 1)^T$. Hence the loop eigenmodes of $\mathcal{H}_{k=1}$ are

$$\begin{aligned} |\Psi_{k=1}(2)\rangle &= \begin{pmatrix} V \\ V \\ V \end{pmatrix}, & |\Psi_{k=1}(-1)\rangle &= \begin{pmatrix} -2V \\ V \\ V \end{pmatrix}, \\ |\Psi_{k=1}(1)\rangle &= \begin{pmatrix} 0 \\ -V \\ V \end{pmatrix}. \end{aligned} \quad (15)$$

The first eigenvector corresponds to $\epsilon_{k=1} = 2\lambda_s = 2$, the second to $\epsilon_{k=1} = -\lambda_s = -1$ and the third one to $\epsilon_{k=1} = \lambda_s = 1$. The sequencing of condensates wavefunctions inside eigenvectors proceeds according to the following notation: $(\psi_1^0 \psi_2^0 \psi_3^0 \psi_1^1 \psi_2^1 \psi_3^1 \psi_1^2 \psi_2^2 \psi_3^2)^T$. The eigenmodes (15) along with their complex conjugates constitute the six loop eigenvectors of the $k=1$ system. The remaining three eigenvectors can be obtained in the same way with V replaced by $|\Psi_{k=0}(-4)\rangle$, but they do not maintain loop supercurrents and we do not consider them here.

Before proceeding to $k=2$ case, we briefly discuss the results (15), schematically presented in Fig. 3. The first eigenvector $|\Psi_{k=1}(2)\rangle$ corresponds to the upper bound of the spectrum $\epsilon = 2$, the energy value with the largest multiplicity⁷ (see Fig. 13). It is a trivial eigenvector since all triangles (large and small in Fig. 3(a)) are equivalent to the three-site ring with circulant current per triangle readily evaluated $I = \sqrt{3}$. We also expect the same stability behavior as in three-site rings once the interaction is turned on (to be discussed in Section IV). We refer to these modes as *standard* hereafter.

The next loop state $|\Psi_{k=1}(-1)\rangle$ is schematically displayed in Fig. 3 (b) and it corresponds to the isolated energy state within the largest gap in the spectrum (see Fig. 13). This mode is different from the standard mode in two ways: the inner triangles have smaller filling factors, expressed by smaller circles; phases of the BECs on the inner triangles are shifted by π with respect to the standard configuration in Fig. 3(a). We show later that this kind of modes will be present in all generations and we will refer to them as *periodic* for reasons explained in Section IV.

Finally, we discuss states corresponding to the gap boundary at $\epsilon = 1$. In this case the Sierpinski gasket is only partially filled as is seen in Fig. 3 (c). The two inner triangles are then essentially uncoupled, but the phases in the upper inner triangle are shifted by π with

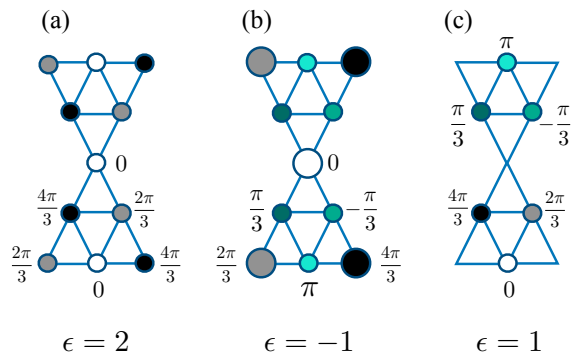


FIG. 3: Schematic representation of loop eigenstates of stage $k = 1$. A circle represents a Bose-Einstein condensate. Circles of the same size correspond to the same filling ρ , such that the filling of all sites in (a) is the same, however, in (b) some of the sites have larger filling factors, shown by larger circles, in (c) some sites are not filled at all. Different colors refer to different phases of condensates, for example, white color means 0-phase, grey - phase $2\pi/3$, bright blue - phase π etc.

respect to the phases of the lower triangle. This is a partially loop state.

B. Loop eigenmodes of $k = 2$ stage

The elegant way of deriving eigenvalues and eigenvectors presented in Sec. III A can not be applied here due to the changed structure of the Hamiltonian. For this reason we should resume to either the hierarchical derivation procedure⁷, briefly outlined in the Appendix B, or to numerics for special values.

We start with the discussion of states corresponding to the spectrum upper boundary $\epsilon = 2$. Out of the nine new cases (see the Flowchart in Fig. 2), only four are of interest since loop eigenmodes come in conjugated pairs. One of the four vectors will be a standard eigenmode of the type shown in Fig. 3(a). This is easy to demonstrate from the structure of the Hamiltonian (see Appendix B for details). The standard modes will therefore be always present in all generations of Sierpinski gasket, representing the highest excited states.

The remaining three eigenmodes for $\epsilon = 2$ are quite convoluted (see Appendix B), we refer to such modes as chaotic and choose to represent them in state space for clarity. In Fig. 4 (a) and (b) we show the associated state spaces for two out of three chaotic modes (this is essentially a representation of the multidimensional fixed point). We color-coded them according to triangles the fixed points (or rather components of the multidimensional fixed point) belong to. The color-coding was motivated by the fact, that at this stage the blue, red and orange subtriangles are not equivalent any more in terms of their fixed points, and as a consequence circular currents will be also different. This kind of behaviour was not observed in stage $k = 1$.

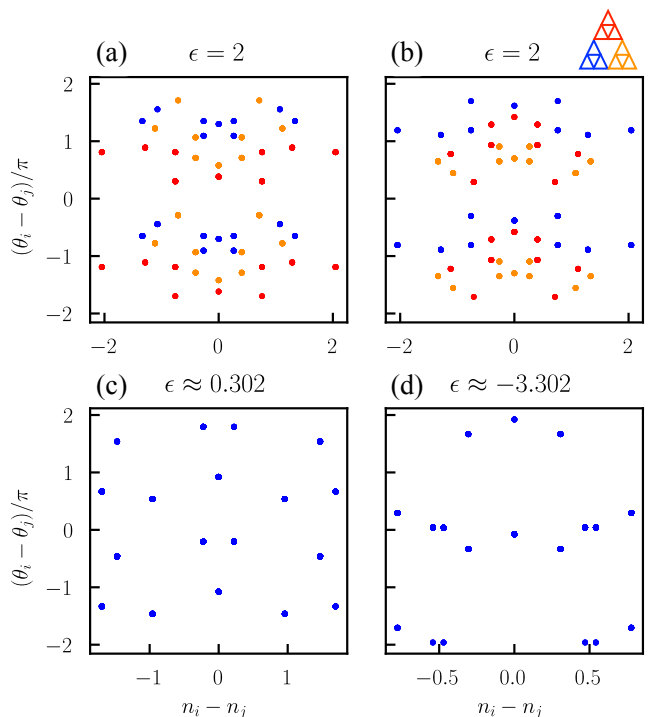


FIG. 4: State space representation of *chaotic* eigenvectors in generation $k = 2$ for different eigenenergies, indicated above the graphs. All phase differences of all nearest neighbors are plotted versus all population differences of all nearest neighbors. The small triangle on the top right explains the color coding within the fixed points corresponding to eigenvectors of (a) and (b). (a) corresponds to $|\psi_2(\epsilon = 2)\rangle_2$, (b) to $|\psi_2(\epsilon = 2)\rangle_3$, (c) to $|\psi_2(\epsilon \approx -3.302)\rangle$ and (d) to $|\psi_2(\epsilon \approx 0.302)\rangle$ (see Appendix B). Blue, red and orange fixed points coincide for (c) and (d).

The last eigenvector from this series $|\psi_2(\epsilon = 2)\rangle_4$ is the same as the one in Fig. 4 (a), but with colors interchanged: blue points turn red, orange ones turn blue and red ones turn orange. We note that associated state spaces for chaotic modes are quite "busy" with fixed points distributed all over the space and occupation differences taking values between 0 and ≈ 2 . In contrast, standard eigenmodes have just one fixed point, because all population differences are the same and equal to zero, whereas all phase differences are equal to $2\pi/3$ (see Fig. 3(a)).

We now proceed to modes derived from "gap" states of the previous stage, i.e. states corresponding to $\epsilon_{k=1} = -1$. Although the asymmetry between the sub-triangles is not present for them, i.e. fixed points for blue, orange and red triangles coincide, the modes are very similar to the chaotic modes for $\epsilon = 2$, in that there is a rather broad distribution of phase differences as well as populations differences (see Fig. 4 (c) and (d)). We place hence the modes in the chaotic class.

Periodic modes in this generation are derived from the standard modes of generation $k = 1$. It turns out (see

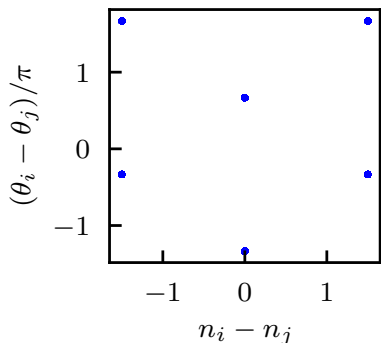


FIG. 5: State space representation of *periodic* eigenvectors, stage independent ($k = 1, 2, \dots$): all phase differences of all nearest neighbors are plotted versus all population differences of all nearest neighbors.

TABLE I: Circular current I of the lower half fractal for stage $k = 2$ and different energies ϵ .

ϵ	I
2 (standard)	$\sqrt{3}$
2 (chaotic)	0
≈ 0.302 (chaotic)	0.184
≈ -3.302 (chaotic)	0.104
-1 (periodic)	$-\frac{\sqrt{3}}{2}$

Appendix B) that in terms of state space representation, the new periodic modes are not different from the old ones: each new triangle will represent a standard ring, but with smaller occupation numbers compared to the triangle it is inserted in. The phases of the new triangle will be shifted by π with respect to its hosting triangle as in Fig. 3(b) and so on. The state space representation of such modes is as a consequence very simple and remains the same for any generation greater than 0 - see Fig. 5.

Finally, the partially filled modes of generation $k = 1$ give rise to partially filled modes of generation $k = 2$ with effectively separated subsystems with loop currents as we show in Appendix B. Since the dimensionless energies of these two new modes are irrational numbers (see Flowchart in Fig. 2), the modes acquire many broadly distributed fixed points within their corresponding subspaces. Since this picture is not principally different from the chaotic modes, we do not elaborate on such modes in the following.

All the loop modes are characterised by constant circular current per triangle, which can be calculated analytically or numerically. The values of the current can be very different, we give a number of examples for the total current in Table I.

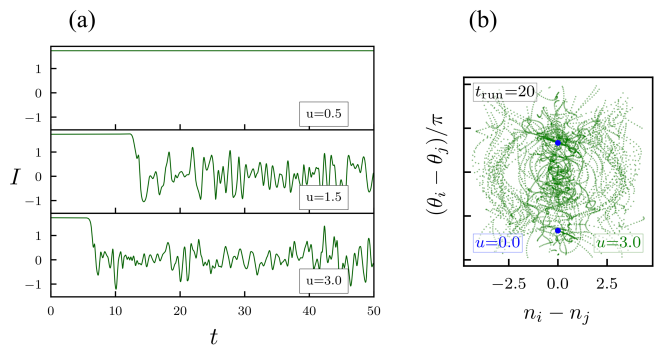


FIG. 6: (a) Circular current I of the lower half fractal versus time (in units of $1/K$) for a standard mode of generation $k = 1$ for different interaction values u . Random deviations of phases and occupations from their eigenmode values of the order of 10^{-8} is introduced. (b) Phase space trajectories for the same mode after time run $t_{\text{run}} = 20$. For $u = 0$ the mode is represented by fixed points shown in blue. For $u \neq 0$ the system becomes chaotic with trajectories covering all the phase space available.

IV. INCLUSION OF INTERACTION AND CHAOS ONSET

In this Section we investigate the role of interaction u in the behaviour of circular current and stability of non-interacting fixed points representing loop eigenmodes discussed in the previous Section. The analysis is mostly done numerically by solving Eqs. (5) with Runge-Kutta method.

A. Standard modes

The standard modes (Fig. 6) are different from all the other modes in that they remain fixed points of the DNLS equations (5) even when interaction is turned on. It means that a circular current calculated along any triangular plaquette remains constant in time for $u \neq 0$. This interesting property is inherited from a standard three-site ring mode with equal populations and phase difference equal to $2\pi/3$ between all pairs of neighboring sites^{41,46}. The stability of the standard mode, however, depends on interaction. In a ring the mode changes from stable to unstable at a critical value $u = u_c = 1.5$, which can be derived analytically from linear stability analysis. In the unstable regime the system can be forced out of the stationary state by a smallest perturbation and circular current plunges into chaotic dynamics, albeit not immediately, but after a period of time t_c which depends on perturbation and interaction⁴⁶. We see this kind of behaviour in Sierpinski gaskets as well, exemplified in Fig. 6. Fig. 6(a) displays the circular current I becoming chaotic with time, whereas Fig. 6(b) presents phase space chaotic trajectories associated with this behaviour.

To understand better this dynamics and to find u_c we perform linear stability analysis of the standard modes

for $k = 1$ and $k = 2$. It is useful to convert to canonical coordinates first. All n_i remain the same except for the one being eliminated through particle conservation, for example the N th coordinate $n_N = N - \sum_{i=1}^{N-1} n_i$. The corresponding phase variables are $P_i = \theta_N - \theta_i$ with $i = 1, \dots, N-1$. The canonical variables satisfy the Hamilton equations of motion $\dot{n}_i = -\frac{\partial H}{\partial P_i}$ and $\dot{P}_i = \frac{\partial H}{\partial n_i}$. The initial condition remains a fixed point in these variables. The Jacobian J of the size $2(N-1)$ then reads

$$J = \begin{pmatrix} \frac{\partial \dot{n}_1}{\partial n_1} & \dots & \frac{\partial \dot{P}_{N-1}}{\partial n_1} \\ \vdots & \ddots & \vdots \\ \frac{\partial \dot{n}_1}{\partial P_{N-1}} & \dots & \frac{\partial \dot{P}_{N-1}}{\partial P_{N-1}} \end{pmatrix} \quad (16)$$

Calculation of its eigenvalues λ_i is carried out numerically and the results for two generations are shown in Fig. 7. We see that indeed, for small u -s all eigenvalues are purely imaginary and the system is stable, i.e. remains in its fixed point. However, once at least one eigenvalue acquires a non-zero real part, the stability is violated. We identify thus that $u_c(k=1) = 0.5$ and $u_c(k=2) = 0.3$. We see that u_c indeed, depends on the generation. This is not very surprising, since the Jacobian is getting larger with each generation, which amounts to a broader distribution of its eigenvalues and therefore more complicated equations for u_c . We expect, that in thermodynamics limit u_c will be tending to zero.

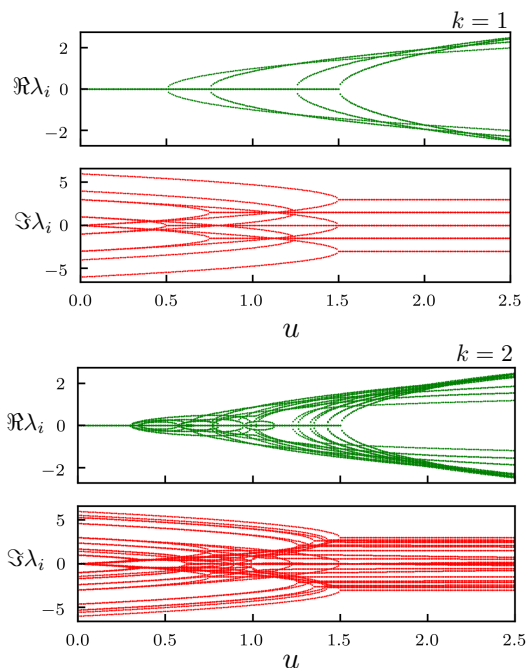


FIG. 7: Real (green) and imaginary (red) parts of all Jacobian eigenvalues λ_i versus the interaction parameter u , for the standard mode in generations $k = 1$ and $k = 2$. u_c is determined by the first λ_i acquiring a non-zero real part.

As discussed, the sliding into a chaotic dynamics does not necessary happens immediately, so that there is a

certain time-scale t_c associated with that. In order to evaluate the time-scale we introduce small random deviations of the phases and occupation numbers of condensates according to

$$\begin{aligned} \theta_i &\rightarrow \theta_i + \delta r_i, \\ n_i &\rightarrow n_i + \delta r_j, \end{aligned} \quad (17)$$

where $r_{i,j}$ are random numbers from $[-1, 1]$, whereas δ is a parameter. We then numerically analyse t_c in dependence of u for different values of δ . The results are presented in Fig. 8. As expected, t_c diverges in the vicinity of u_c , found from linear stability analysis, and decreases with the growth of u . If one fixes u , then the characteristic time rapidly decreases as the deviation δ from the stationary value becomes larger.

Interestingly, t_c for the standard mode of generation $k = 2$ has an additional kink at about $u \approx 0.7$. We attribute the kink to the unusual behaviour of the Jacobian eigenvalues λ_i around this value of u . As can be seen in Fig. 7 some of the real parts go back to zero around this value of u , thus trying to force the system back into a stationary state. This is reflected in the increased t_c in the interval $u \in [u_c, 0.7)$ for $k = 2$.

B. Chaotic modes

Chaotic modes shown in Fig. 4 appear only in the second generation of Sierpinski fractal and are characterised by components of their fixed point distributed all over the phase space. Since these modes are not fixed points of the interacting system, circular currents associated with them become immediately chaotic once the interaction is on. This behaviour is demonstrated in Fig. 9, where we show one of the chaotic modes for $\epsilon = 2$ (Figs. a) and b)) and a mode for $\epsilon = -3.302$ (Figs. c) and d)).

Figs. a) and c) depict phase space trajectories for $u = 5$ after a certain time-run $t_{run} = 10$. We see that in a) the system evolves all over the phase space, a behaviour characteristic of chaotic dynamics. In Fig. 9 b) the total current turns indeed chaotic for the interacting system signalling the immediate loss of coherence between BECs.

Figs. 9 c) and d) demonstrate that, interestingly, the $\epsilon = -3.302$ -mode first undergoes a weakly-chaotic regime characterised by the circular currents oscillating around their stationary values. In the projected phase portrait this is reflected in semi-elliptic trajectories of the system close to some of the components of the fixed point (see Fig. 9(c)). Remarkably, this weak chaotic regime does not last forever but is associated with a time scale, similar to the standard mode behaviour in that it decreases with the growth of u . We attribute this fascinating behaviour to the nonhomogenous distribution of the fixed point components in such a mode. Specifically, we mean the quasi-isolated bunch of components concentrated in the narrow interval around $(\theta_i - \theta_j)/\pi = 0$ and rather broadly distributed in $n_i - n_j$. The time-scale t_c is an

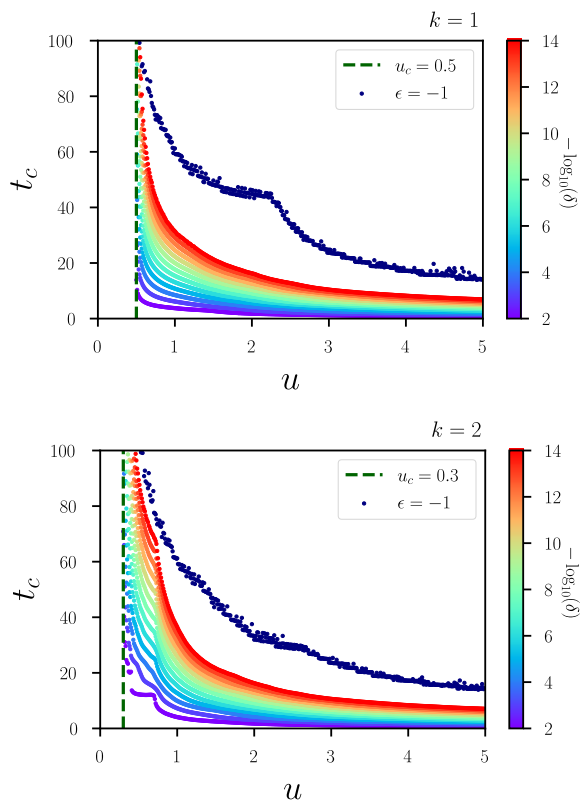


FIG. 8: Critical time t_c (in units $1/K$) in dependence of interaction u for the standard mode of generations $k = 1$ and $k = 2$. The scaling parameter δ of the initial phase and occupation displacement is varied from 10^{-2} to 10^{-14} . Critical interaction derived from linear stability analysis is shown by the vertical dashed line for convenience. t_c of a periodic mode (i.e. a mode for $\epsilon = -1$) is shown for comparison with dark blue dots.

effective time period necessary for this quasi-isolated subspace to get connected with other subspaces, which inevitably happens when a system is chaotic. For example, for the case in Fig. 9 d) $t_c \approx 30$. This time period is getting shorter with increased interaction as one would expect.

C. Periodic modes

Finally, we discuss the periodic modes, i.e. modes corresponding to $\epsilon = -1$, which have the same state space representation in all generations for $u = 0$. Similar to chaotic modes, these eigenstates do not remain fixed points in interacting system. However, cyclic supercurrents associated with these modes do not turn chaotic immediately either when $u \neq 0$. Instead, they undergo a temporary regime, where all supercurrents manifest periodic behaviour.

We first examine this periodic dynamics for different values of u . In Fig. 10 (a) and (c) we show how the total current oscillations change with increasing u . Interest-

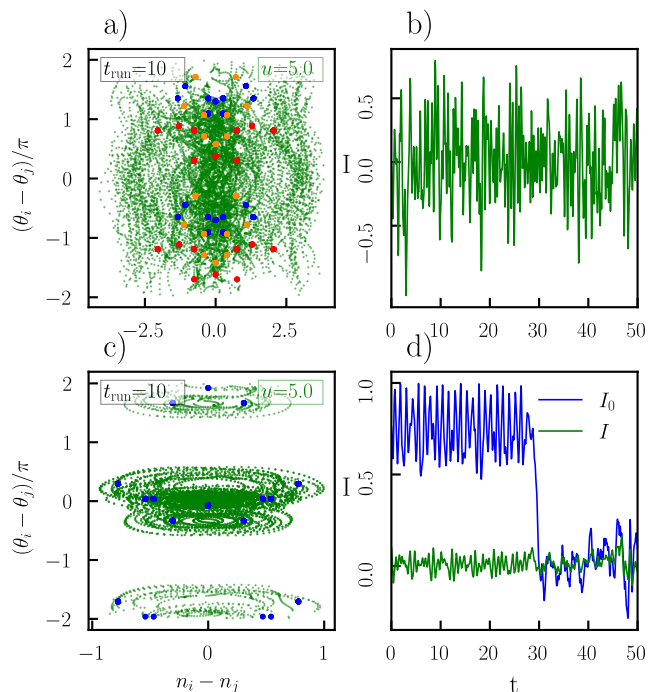


FIG. 9: Chaotic modes for $u \neq 0$, (a) and (c) are the phase space trajectories and (b) and (d) are circular currents. The upper two graphs correspond to energy $\epsilon = 2$, the lower ones to $\epsilon \approx -3.302$. Run time and interaction parameter are $t_{run} = 10$ and $u = 5.0$ for both cases. I is the total current while I_0 is the current along outer triangle only.

ingly, in all cases the current oscillates exactly above its noninteracting value, indicated by the straight blue line. The oscillations contain more than one frequency, which prompted us to perform Fourier analysis of the dynamics, which will be considered later in the text.

In Fig. 10(b) we demonstrate the phase portrait of our system prior to chaos onset. This is the plot for $k = 1$, however we obtained an identical graph for $k = 2$ and hence assume this behaviour is typical of such modes in any generation. In Fig. 10 (b) one notices that dynamics crucially changes when u exceeds a certain value $u_{ST} = 12$. One can observe that for $u < u_{ST}$ the system progresses along closed almost elliptic trajectories. Closed trajectories mean that both phase differences as well as population differences oscillate around some values. This ceases to be the case when u exceeds u_{ST} . Although population differences continue to oscillate around some nonzero values, the phase differences stop oscillating and turn instead into running phases. The transition to running phase regime, termed self-trapping, was originally found in bosonic Josephson junctions of just two coupled condensates³⁷.

The transition to self-trapping at $u = u_{ST} = 12$ is also evident from Fourier analysis of the total circular current presented in Fig. 11. Prior to u_{ST} the current

is characterised by a multi-frequency dynamics with the frequencies only weakly dependent on u . Above u_{ST} one can clearly distinguish three frequencies, which rapidly increase with u . In the upper graph of Fig. 11 minimum and maximum values of the total current are shown in dependence of u in the time window $t \in [0, 10]$. Although minimum value stays interaction independent unless the system enters chaotic regime, the maximum value is linearly-dependent on u in the non-self-trapped case and almost constant or slightly decreasing in the self-trapped regime. Qualitative differences in oscillations and their Fourier transforms before and after self-trapping were also found in bosonic Josephson junctions³³.

In addition to this analysis, we also find fixed points of the system when interaction u is finite. As can be seen from the phase portrait in Fig. 3(b) there are two types of contributions to these fixed points: along the $n_i - n_j = 0$ - line and $n_i - n_j \neq 0$ with $\theta_i - \theta_j = -\pi/3 \pm 2\pi k$. The $n_i - n_j = 0$ ones do not depend on interaction, whereas the latter do. Thus this multidimensional fixed point is characterised just by two occupancies: n and n' ($n \neq n'$). n are the occupancies of the outer triangles shown in white, gray and black colors in Fig. 3(b), and n' are populations of the remaining sites. An equation which relates n , n' and u at stable fixed points can be readily found:

$$-u(n - n') + 2\sqrt{\frac{n'}{n}} - \sqrt{\frac{n}{n'}} + 1 = 0. \quad (18)$$

Using the normalisation condition $n + 2n' = 3$ we can express interaction at the fixed point u^* in terms of n'

$$\frac{1}{3(1 - n')} \left(1 + \frac{4n' - 3}{\sqrt{(3 - 2n')n'}} \right) = u^*. \quad (19)$$

The analysis of this equation shows that

$$\lim_{u^* \rightarrow \infty} n' = 1_-, \quad \lim_{u^* \rightarrow \infty} n = 1_+ \quad (20)$$

with the noninteracting values being $n'(u = 0) = 1/2$ and $n(u = 0) = 2$. It means that with increasing u the fixed point is moving towards $n_i - n_j = 0$, but never reaches it (we added some of the interaction-dependent fixed points to Fig. 10(b) for $u = 3$, $u = 10$ and $u = 13$). Due to these peculiarities, the trajectories around the fixed points in Fig. 10(b) are never perfect ellipses, but rather egg-shaped.

We note that in a bosonic Josephson junction of cold atoms all fixed points are stable for $u = 0$. It is due to a supercritical pitchfork bifurcation occurring for certain values of u , that one of the fixed points changes its character to unstable³³. This change eventually leads to self-trapping. In contrast, our system is characterised by a multidimensional unstable fixed point, whose number of components does not change with interaction. This fixed point can be effectively described with two components: one stable and one unstable, as is clearly seen in the projected phase portrait in Fig. 10. It is the tendency

of the stable component of the fixed point to align with the unstable one along $n_i - n_j = 0$ - line with increasing interaction, which eventually causes the self-trapping.

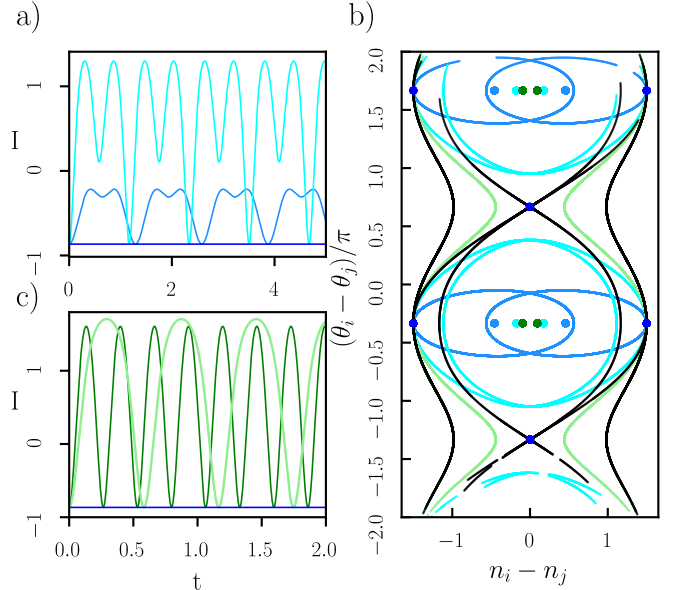


FIG. 10: Periodic modes for $u \neq 0$. (b) presents the phase space trajectories for different values of u : $u = 3$ (dark blue), $u = 10$ (light blue), $u = 12$ (black), $u = 13$ (light green), $u = 20$ (dark green), the dots of the same color represent corresponding fixed points calculated from Eq. (19). The bright blue dots are the same as in Fig. 5. (a) and (c) show the currents associated with these interaction values the prior for $u < 12.0$, the latter for $u > 12.0$. There is a qualitative change at the self-trapping critical interaction $u_{ST} = 12.0$. All currents exclusively oscillate above the non-interacting value. The run time for (a) is set to $t_{run} = 5$ in order to not include the chaotic regime.

Another difference with a bosonic Josephson junction, is that the oscillating dynamics of the periodic modes transforms after a while into chaotic. This is exemplified in Fig. 12 where the total cyclic current is shown versus time for $u = 3$. The characteristic time scale associated with chaotic dynamics t_c is not easy to evaluate numerically due to obstructing oscillations. We therefore define a condition for the onset of chaos by first fitting the linear rise in amplitude from the upper part of Fig. 11, resulting in:

$$I_{Max} = 0.220(\pm 0.000) \cdot u - 0.878(\pm 0.001). \quad (21)$$

The value of the intercept should be the current value for the non-interacting case, $-\sqrt{3}/2 \approx -0.866$, the discrepancy could be attributed to the first few I_{Max} values deviating from the linear curve more than any others. From these findings a condition for estimating t_c can be formulated: if the current either exceeds the I_{Max} curve or goes below the minimum value by a certain margin (in this case 0.05) the time is taken as the critical one for that

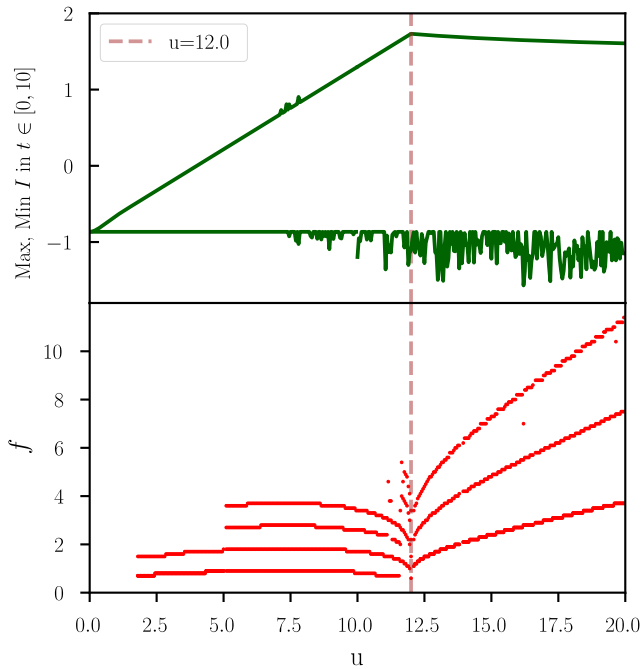


FIG. 11: In the upper graph the maximum and minimum values of the total current during $t_{\text{run}} = 10$ versus interaction are shown (for a periodic mode). Signs of chaotic behaviour are present for $u > 7.5$. The lower graph depicts the biggest frequency contributions to the circular current of periodic modes in dependence of interaction. For the latter the frequencies of the largest detectable contributions to the Fourier transform are shown. Only values above $u = 1.75$ are considered since the oscillations of the current below this value are very small and difficult to detect. Above $u = 5.0$ two more frequency contributions can be detected. Around u_{ST} there is noise due to difficulty in properly detecting frequencies.

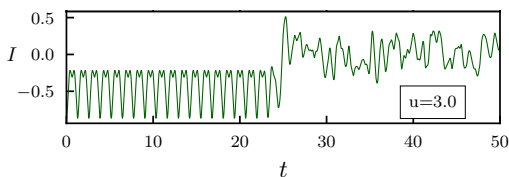


FIG. 12: The total circular current I of a periodic mode for $u = 3$, $k = 2$. The dynamics changes from periodic to chaotic at $t_c \approx 25$.

u . This of course only applies to interaction values below $u = 12.0$. The corresponding graph is presented in Fig. 8, once again t_c falls with rising interaction parameter, however the $k = 1$ case shows a pronounced kink. Since linear stability analysis is not applicable in this case, we can not make a conclusion about the origins of the kink.

V. CONCLUSIONS AND DISCUSSION

In this work we provide a detailed and systematic analysis of eigenmodes carrying loop currents in a system of weakly-interacting condensed bosons in Sierpinski gaskets. In a noninteracting system we identify energy levels which can accommodate such eigenstates and find those states analytically where possible, or numerically. It turns out the loop states can be very different in the distribution of their site populations as well as phase differences between nearest neighbors, often counter-intuitive. To make our main results more transparent we divide the discovered modes into three main classes: standard, chaotic and periodic.

Standard modes correspond to the spectrum upper boundary and are very similar in behaviour to the dynamics of the basic unit of Sierpinski gasket - a simple three-site ring. They appear in all generations of Sierpinski gasket and become unstable for certain finite values of u for small gaskets with $u_c \rightarrow 0$ for larger systems.

Chaotic loop modes can appear for highly degenerate spectrum upper boundary, as well for irrational eigenenergies (all energies expressed in the units of coupling constant K). These modes appear first time at the stage $k = 2$ and we assume them to be typical of fractal lattices. One would not expect such modes in a regular lattice.

We also identify modes, which we refer to as periodic. These modes are stationary states which are characterised by two contributions to the fixed point (due to symmetric phase space this suffices). One of them has zero occupation difference and remains where it is in the phase space even when the interaction is turned on. The other (for a different phase difference and nonzero population imbalance) changes the occupation difference with interaction strength. Thus the $u = 0$ initial condition is no longer a fixed point and undergoes periodic dynamics. As we know from simple pendulums, this kind of constellation of fixed points in a phase space can lead to running phase modes, termed macroscopic self-trapping in the context of Bose Josephson junctions. And this is indeed what happens for the periodic modes with increasing interaction. Interestingly, this behaviour due to self-similarity of the modes, is expected at all generations $k \geq 1$ of Sierpinski gasket.

All in all, these are novel and unexpected results, which motivate further studies of these intriguing systems. For example, modes for $k = 1$ and $\epsilon = 1$ resemble edge modes in fractal photonic insulators³ and deserve further exploration.

Another line of research could be a generalisation to driven lattices, which is important because the driving force could account for the effect of gravitational field. At least for quasi-one-dimensional lattices of condensates the mean-field dynamics was in an excellent agreement with experiments probing full quantum many-body behaviour¹⁸. Since chaotic dynamics seems to be a natural attribute of systems of coupled condensates, would be

instructive to measure its characteristics experimentally, for example, by Loschmidt echo methods, suggested in³⁹.

Finally, the role of quantum fluctuations and study of possible thermalisation of bosons in fractal lattices could give researchers further clues about the role of chaos and eigenstate thermalisation hypothesis^{6,21,38}, as well as dynamical heat bath generation mechanisms^{31,32}.

Appendix A: Spectrum of the noninteracting system

Here we briefly outline the main results for the single-particle spectrum derived in Refs.^{7,34}. The spectrum was calculated with the help of a decimation procedure according to which the Hamiltonian of generation k is mapped onto the Hamiltonian of the previous generation $k - 1$. The procedure works consistently provided each site of a lattice is connected to the same number of nearest neighbors, in our case to the four nearest sites. In this case the basic structure of the effective Hamiltonian (the one defined on a subspace of "old" sites) does not change with on-site energies and effective coupling being renormalized in a simple way. To secure this requirement, periodic boundary conditions were suggested in⁷, also shown in Fig. 1. This allowed to calculate the spectrum of infinite Sierpinski gasket. The spectrum is bounded, discrete and highly degenerate.

As a result of the renormalization procedure, eigenenergies of generation k fractal can be expressed recursively in terms of eigenenergies of the previous generation $k - 1$ (in the units of K)

$$\epsilon_{k,\pm} = \frac{-3 \pm \sqrt{(9 - 4 \cdot \epsilon_{k-1})}}{2}. \quad (22)$$

This recursion does not, however, account for all values of possible eigenenergies. There are three exceptional values $\epsilon^* = \pm 2; 1$, which should be treated separately (for these values the renormalization scheme fails, leading to either singularities or zeros in renormalized effective energies⁷). If one disregards the special values ϵ^* for the moment, one can analyse the stability of the recursive relation (22), and show that a sequence of spectral gaps is generated out of it in a regular manner. This sequence of gaps is in turn, a fractal described by a Cantor set of Lebesgue measure zero^{7,34}.

The whole spectrum as a result contains three parts: the special values, values inside the gap intervals, values directly at the edges of the gaps. Values inside the gaps originate from $\epsilon = 2$. Values at the gap edges descend from $\epsilon = 1$. The entire spectrum is then a point set of Lebesgue measure zero⁷. The multiplicities of all values, special or not, are not difficult to calculate and as a result density of states for Sierpinski gasket of any size can be produced⁷. For convenience we reproduce here the density of states (DOS) for the first 10 generations of Sierpinski gasket (see Fig. 13). We will refer to this DOS later in the text. Note, that DOS exhibits self-similarity properties as well⁷.

Appendix B: Details of hierarchical derivation of eigenvectors for $k = 1$ and $k = 2$

The idea of hierarchical derivation was outlined in Ref.⁷. Here we give an example of how the decimation procedure works for $k = 1$. The eigenvalue problem for

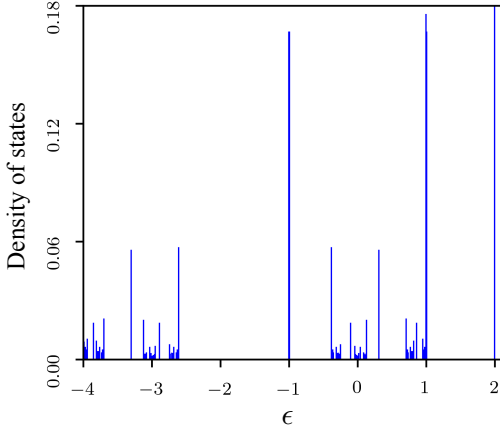


FIG. 13: Density of states for the first 10 generations of Sierpinski gasket. Such density of states was first presented in⁷. The peak at $\epsilon = 2$ is very high due to the large degeneracy of the eigenvalue, so we cut it at 0.18.

an eigenstate $|\Psi\rangle$ in generation k is formulated in a two-dimensional space $\{|\Psi_1\rangle, |\Psi_2\rangle\}$, where $|\Psi_1\rangle$ is the projection of $|\Psi\rangle$ onto the "old" subspace - the subspace of generation $k - 1$, whereas $|\Psi_2\rangle$ is the the projection of $|\Psi\rangle$ onto the "new" subspace, the one comprising all the "new" sites which were added in generation k . The Schrödinger equation in then

$$\begin{pmatrix} \mathcal{H}_{11} & \mathcal{H}_{12} \\ \mathcal{H}_{21} & \mathcal{H}_{22} \end{pmatrix} \begin{pmatrix} |\psi_1\rangle \\ |\psi_2\rangle \end{pmatrix} = \epsilon \begin{pmatrix} |\psi_1\rangle \\ |\psi_2\rangle \end{pmatrix}. \quad (23)$$

For example, if we are at stage $k = 1$, then we partition our Hamiltonian (13) in the following way

$$\begin{aligned} H_{11} &= \hat{0}, \\ H_{12} &= (H_{21})^T = (\hat{S} \hat{S}) \\ H_{22} &= \begin{pmatrix} \hat{S} & \hat{0} \\ \hat{0} & \hat{S} \end{pmatrix}. \end{aligned} \quad (24)$$

Now we can express the new eigenvectors $|\psi_2\rangle$ in terms of the old states $|\psi_1\rangle$

$$|\psi_2\rangle = (\epsilon \hat{\mathbb{I}} - \mathcal{H}_{22})^{-1} \mathcal{H}_{21} |\psi_1\rangle. \quad (25)$$

Since H_{22} is always block-diagonal with blocks equal to \hat{S} , it is easy to invert the matrix $(\epsilon \hat{\mathbb{I}} - \mathcal{H}_{22})$ just by inverting each block

$$\begin{aligned} (\epsilon \hat{\mathbb{I}} - \hat{S})^{-1} &= \frac{1}{\epsilon^2 + \epsilon - 2} \begin{pmatrix} 1 + \epsilon & -1 & -1 \\ -1 & 1 + \epsilon & -1 \\ -1 & -1 & 1 + \epsilon \end{pmatrix} = \\ &= \frac{1}{\epsilon^2 + \epsilon - 2} ((1 + \epsilon)\hat{\mathbb{I}} + \hat{S}) \equiv \hat{B}. \end{aligned} \quad (26)$$

For example, we want to calculate an eigenvector, generated by $|\psi_1\rangle = V$ from Eq. (12). V corresponds to the eigenvalue $\epsilon_{k=0} = 2$, in the generation $k = 1$ this

eigenvalues generates $\epsilon_{k=1} = -1$ (see Fig. 2), therefore $\epsilon = -1$ in Eqs. (25) and (26). After some algebra we get

$$(\epsilon \hat{\mathbb{I}} - \mathcal{H}_{22})^{-1} \mathcal{H}_{21} = - \begin{pmatrix} 1 & 0.5 & 0.5 \\ 0.5 & 1 & 0.5 \\ 0.5 & 0.5 & 1 \end{pmatrix}. \quad (27)$$

Now from Eq. (25) we get

$$|\psi_2\rangle = \begin{pmatrix} -1/2 \\ (-i\sqrt{3} + 1)/4 \\ (i\sqrt{3} + 1)/4 \\ -1/2 \\ (-i\sqrt{3} + 1)/4 \\ (i\sqrt{3} + 1)/4 \end{pmatrix} = \begin{pmatrix} -0.5 \\ 0.5e^{-i\pi/3} \\ 0.5e^{i\pi/3} \\ -0.5 \\ 0.5e^{-i\pi/3} \\ 0.5e^{i\pi/3} \end{pmatrix}, \quad (28)$$

so that

$$|\Psi\rangle = \begin{pmatrix} |\psi_1\rangle \\ |\psi_2\rangle \end{pmatrix} = \begin{pmatrix} 1 \\ e^{i2\pi/3} \\ e^{i4\pi/3} \\ -0.5 \\ 0.5e^{-i\pi/3} \\ 0.5e^{i\pi/3} \\ -0.5 \\ 0.5e^{-i\pi/3} \\ 0.5e^{i\pi/3} \end{pmatrix} \quad (29)$$

which is equivalent to $|\Psi_{k=1}(-1)\rangle$ in Eq. (15).

In the next stage $k = 2$ the partitioned Hamiltonian has the following blocks: H_{11} is a 9×9 matrix of zeros, H_{22} is a 6×6 block-diagonal matrix with blocks \hat{S} on its main diagonal, so that $(\epsilon \hat{\mathbb{I}} - \mathcal{H}_{22})^{-1}$ is a block-diagonal matrix with each block equal to \hat{B} from Eq. (26). For H_{21} we get

$$H_{21} = - \begin{pmatrix} \hat{B}_1 & \hat{B}_2 & \hat{0} \\ \hat{B}_3 & \hat{B}_4 & \hat{0} \\ \hat{B}_5 & \hat{B}_6 & \hat{0} \\ \hat{B}_1 & \hat{0} & \hat{B}_2 \\ \hat{B}_3 & \hat{0} & \hat{B}_4 \\ \hat{B}_5 & \hat{0} & \hat{B}_6 \end{pmatrix}, \quad (30)$$

where

$$\begin{aligned} \hat{B}_1 &= \begin{pmatrix} 0 & 0 & 0 \\ 1 & 0 & 0 \\ 1 & 0 & 0 \end{pmatrix}, \hat{B}_2 = \begin{pmatrix} 0 & 1 & 1 \\ 0 & 0 & 1 \\ 0 & 1 & 0 \end{pmatrix}, \\ \hat{B}_3 &= \begin{pmatrix} 0 & 1 & 0 \\ 0 & 0 & 0 \\ 0 & 1 & 0 \end{pmatrix}, \hat{B}_4 = \begin{pmatrix} 0 & 0 & 1 \\ 1 & 0 & 1 \\ 1 & 0 & 0 \end{pmatrix}, \\ \hat{B}_5 &= \begin{pmatrix} 0 & 0 & 1 \\ 0 & 0 & 1 \\ 0 & 0 & 0 \end{pmatrix}, \hat{B}_6 = \begin{pmatrix} 0 & 1 & 0 \\ 1 & 0 & 0 \\ 1 & 1 & 0 \end{pmatrix}, \end{aligned} \quad (31)$$

so that

$$(\epsilon \hat{\mathbb{I}} - \mathcal{H}_{22})^{-1} \mathcal{H}_{21} = - \begin{pmatrix} \hat{B} \cdot \hat{B}_1 & \hat{B} \cdot \hat{B}_2 & 0 \\ \hat{B} \cdot \hat{B}_3 & \hat{B} \cdot \hat{B}_4 & 0 \\ \hat{B} \cdot \hat{B}_5 & \hat{B} \cdot \hat{B}_6 & 0 \\ \hat{B} \cdot \hat{B}_1 & 0 & \hat{B} \cdot \hat{B}_2 \\ \hat{B} \cdot \hat{B}_3 & 0 & \hat{B} \cdot \hat{B}_4 \\ \hat{B} \cdot \hat{B}_5 & 0 & \hat{B} \cdot \hat{B}_6 \end{pmatrix}. \quad (32)$$

It can be now easily shown that the vector $(V, V, V)^T$

from stage $k = 1$ will generate $|\Psi_2\rangle = (V, V, V, V, V, V)^T$ and therefore a standard eigenvector of the type depicted in Fig. 3(a). This will be one of the eigenvectors for $\epsilon_{k=2} = 2$. The remaining three can be calculated only numerically. Here we present only the $|\Psi_2\rangle$ part of them in order to save space (the vectors are then appended by $|\Psi_1\rangle = (VVV)^T$):

$$|\psi_2(\epsilon = 2)\rangle_2 = \begin{pmatrix} 1.440 \\ 0.5 + 0.342 \cdot i \\ -0.5 - 0.342 \cdot i \\ -0.163 + 0.283 \cdot i \\ 1.103 + 0.059 \cdot i \\ -0.603 - 0.925 \cdot i \\ 0.133 - 0.230 \cdot i \\ -0.307 - 0.754 \cdot i \\ 0.807 - 0.112 \cdot i \\ 0.030 + 0.814 \cdot i \\ -0.796 - 0.171 \cdot i \\ -0.204 + 0.171 \cdot i \\ -1.016 - 0.433 \cdot i \\ 0.25 + 1.076 \cdot i \\ 0.25 - 0.210 \cdot i \\ -0.424 - 0.433 \cdot i \\ 0.25 - 0.552 \cdot i \\ 0.25 + 1.418 \cdot i \end{pmatrix}, |\psi_2(\epsilon = 2)\rangle_3 = \begin{pmatrix} -0.266 \\ -0.5 - 0.643 \cdot i \\ -0.5 + 0.643 \cdot i \\ -0.720 - 1.247 \cdot i \\ -0.046 + 0.604 \cdot i \\ 0.546 + 0.262 \cdot i \\ -0.163 - 0.283 \cdot i \\ 1.103 - 0.059 \cdot i \\ -0.603 + 0.925 \cdot i \\ 0.883 + 0.663 \cdot i \\ -1.057 + 0.321 \cdot i \\ 0.057 - 0.321 \cdot i \\ -0.424 + 0.433 \cdot i \\ 0.25 + 0.552 \cdot i \\ 0.25 - 1.418 \cdot i \\ 0.690 + 0.433 \cdot i \\ 0.25 - 0.775 \cdot i \\ 0.25 - 0.091 \cdot i \end{pmatrix}, |\psi_2(\epsilon = 2)\rangle_4 = \begin{pmatrix} 0.326 \\ -0.5 - 0.985 \cdot i \\ -0.5 + 0.985 \cdot i \\ 0.133 - 0.230 \cdot i \\ -0.307 - 0.754 \cdot i \\ 0.807 - 0.112 \cdot i \\ -0.720 + 1.247 \cdot i \\ -0.046 - 0.604 \cdot i \\ 0.546 - 0.262 \cdot i \\ 0.587 - 0.150 \cdot i \\ 0.353 + 0.492 \cdot i \\ -1.353 - 0.492 \cdot i \\ 0.690 - 0.433 \cdot i \\ 0.25 + 0.775 \cdot i \\ 0.25 + 0.091 \cdot i \\ -1.016 - 0.433 \cdot i \\ 0.25 + 1.076 \cdot i \\ 0.25 - 0.210 \cdot i \end{pmatrix}.$$

We now discuss loop eigenmodes generated from the modes of type Fig. 3 (a). In generation $k = 2$ they will correspond to the eigenvalue $\epsilon = -1$. It means the modes will be moved from the spectrum upper bound to the states within the gap. In order to calculate the new modes we put $\epsilon = -1$ and $|\psi_1\rangle = (V, V, V)^T$ in Eq. (25). When we multiply the matrix of Eq. (32) with $|\psi_1\rangle = (V, V, V)^T$ we get a very simple result

$$|\psi_2\rangle = -\frac{1}{2}(V, V, V, V, V, V)^T, \quad (33)$$

because

$$\begin{aligned} \hat{B} \cdot \hat{B}_1 + \hat{B} \cdot \hat{B}_2 &= \hat{B} \cdot \hat{B}_3 + \hat{B} \cdot \hat{B}_4 = \hat{B} \cdot \hat{B}_5 + \hat{B} \cdot \hat{B}_6 = \\ &= \frac{1}{2} \hat{S}(\hat{B}_1 + \hat{B}_2) = \frac{1}{2} \hat{S}^2. \end{aligned} \quad (34)$$

These eigenmodes hence preserve the structure of the gap modes in Fig. 3(b) with smaller triangles having smaller occupation numbers and phase shifted by π with respect to bigger triangles they are inserted in.

We now analyse states for the eigenvalues $\epsilon \approx -0.381$ and $\epsilon \approx -2.618$. According to the flowchart in Fig. 2

they are derived from partially filled states of generation $k = 1$, it means $|\psi_1\rangle = (0, -V, V)^T$. This leads to

$$|\Psi_2\rangle = \begin{pmatrix} \hat{B} \cdot \hat{B}_2 \cdot V \\ \hat{B} \cdot \hat{B}_4 \cdot V \\ \hat{B} \cdot \hat{B}_6 \cdot V \\ -\hat{B} \cdot \hat{B}_2 \cdot V \\ -\hat{B} \cdot \hat{B}_4 \cdot V \\ -\hat{B} \cdot \hat{B}_6 \cdot V \end{pmatrix}. \quad (35)$$

Since, for example,

$$\hat{B} \cdot \hat{B}_2 \cdot V = \begin{pmatrix} -\epsilon \\ -2e^{i2\pi/3} + \epsilon e^{-i2\pi/3} \\ -2e^{-i2\pi/3} + \epsilon e^{i2\pi/3} \end{pmatrix} \quad (36)$$

and ϵ is an irrational number, the entries of this vector can not be simplified to a "nice" Euler form, with argument being just a rational fraction of π . What we see is that the sites which were unfilled in Fig. 3(c) remain unfilled, thus effectively splitting the fractal into two independent subspaces.

Finally, we derive the eigenmodes corresponding to $\epsilon \approx 0.302$ and $\epsilon \approx -3.302$. In this case $|\psi_1\rangle = (-2V, V, V)^T$,

so that

$$|\Psi_2\rangle = \begin{pmatrix} (2\hat{B} \cdot \hat{B}_1 - \hat{B} \cdot \hat{B}_2)V \\ (2\hat{B} \cdot \hat{B}_3 - \hat{B} \cdot \hat{B}_4)V \\ (2\hat{B} \cdot \hat{B}_5 - \hat{B} \cdot \hat{B}_6)V \\ (2\hat{B} \cdot \hat{B}_1 - \hat{B} \cdot \hat{B}_2)V \\ (2\hat{B} \cdot \hat{B}_3 - \hat{B} \cdot \hat{B}_4)V \\ (2\hat{B} \cdot \hat{B}_5 - \hat{B} \cdot \hat{B}_6)V \end{pmatrix}, \quad (37)$$

$$|\psi_2(\epsilon \approx -3.302)\rangle = \begin{pmatrix} 0.651 \\ 0.826 + 0.101 \cdot i \\ 0.826 - 0.101 \cdot i \\ -0.326 + 0.765 \cdot i \\ -0.326 + 0.564 \cdot i \\ -0.5 + 0.665 \cdot i \\ -0.326 - 0.765 \cdot i \\ -0.5 - 0.665 \cdot i \\ -0.326 - 0.564 \cdot i \end{pmatrix}, |\psi_2(\epsilon \approx 0.302)\rangle = \begin{pmatrix} -1.151 \\ -0.076 + 0.621 \cdot i \\ -0.076 - 0.621 \cdot i \\ 0.576 + 0.245 \cdot i \\ 0.576 - 0.997 \cdot i \\ -0.5 - 0.376 \cdot i \\ 0.576 - 0.245 \cdot i \\ -0.5 + 0.376 \cdot i \\ 0.576 + 0.997 \cdot i \end{pmatrix}.$$

-
- ¹ AIDELSBURGER, M., ATALA, M., LOHSE, M., BARREIRO, J. T., PAREDES, B., AND BLOCH, I. Realization of the Hofstadter hamiltonian with ultracold atoms in optical lattices. *Phys. Rev. Lett.* *111* (Oct 2013), 185301.
- ² ANANIKIAN, D., AND BERGEMAN, T. Gross-Pitaevskii equation for Bose particles in a double-well potential: Two-mode models and beyond. *Phys. Rev. A* *73* (Jan 2006), 013604.
- ³ BIESENTHAL, T., MACZEWSKY, L. J., YANG, Z., KREMER, M., SEGEV, M., SZAMEIT, A., AND HEINRICH, M. Fractal photonic topological insulators. *Science* *376*, 6597 (2022), 1114–1119.
- ⁴ BRZEZIŃSKA, M., COOK, A. M., AND NEUPERT, T. Topology in the Sierpiński-Hofstadter problem. *Phys. Rev. B* *98* (Nov 2018), 205116.
- ⁵ COOKSON, T., KALININ, K., SIGURDSSON, H., TÖPFER, J. D., ALYATKIN, S., SILVA, M., LANGBEIN, W., BERLOFF, N. G., AND LAGOUKAKIS, P. G. Geometric frustration in polygons of polariton condensates creating vortices of varying topological charge. *Nature Communications* *12*, 1 (2021), 2120.
- ⁶ DEUTSCH, J. M. Quantum statistical mechanics in a closed system. *Phys. Rev. A* *43* (Feb 1991), 2046–2049.
- ⁷ DOMANY, E., ALEXANDER, S., BENSIMON, D., AND KADANOFF, L. P. Solutions to the Schrödinger equation on some fractal lattices. *Phys. Rev. B* *28* (Sep 1983), 3110–3123.
- ⁸ DUBERTRAND, R., AND MÜLLER, S. Spectral statistics of chaotic many-body systems. *New Journal of Physics* *18*, 3 (mar 2016), 033009.
- ⁹ DUPONT, N., CHATELAIN, G., GABARDOS, L., ARNAL, M., BILLY, J., PEAUDECFERF, B., SUGNY, D., AND GUÉRY-ODELIN, D. Quantum State Control of a Bose-Einstein Condensate in an Optical Lattice. *PRX Quantum* *2* (Oct 2021), 040303.
- ¹⁰ DZIARMAGA, J., SMERZI, A., ZUREK, W. H., AND BISHOP, A. R. Dynamics of Quantum Phase Transition in an Array of Josephson Junctions. *Phys. Rev. Lett.* *88* (Apr 2002), 167001.
- ¹¹ ENGL, T., DUJARDIN, J., ARGÜELLES, A., SCHLAGHECK, P., RICHTER, K., AND URBINA, J. D. Coherent backscattering in Fock space: A signature of quantum many-body interference in interacting bosonic systems. *Phys. Rev. Lett.* *112* (Apr 2014), 140403.
- ¹² FAN, J. A., YEO, W.-H., SU, Y., HATTORI, Y., LEE, W., JUNG, S.-Y., ZHANG, Y., LIU, Z., CHENG, H., FALGOUT, L., BAJEMA, M., COLEMAN, T., GREGOIRE, D., LARSEN, R. J., HUANG, Y., AND ROGERS, J. A. Fractal design concepts for stretchable electronics. *Nature Communications* *5*, 1 (2014), 3266.
- ¹³ FISHER, M. P. A., WEICHMAN, P. B., GRINSTEIN, G., AND FISHER, D. S. Boson localization and the superfluid-insulator transition. *Phys. Rev. B* *40* (Jul 1989), 546–570.
- ¹⁴ FREMLING, M., VAN HOOFT, M., SMITH, C. M., AND FRITZ, L. Existence of robust edge currents in Sierpiński fractals. *Phys. Rev. Res.* *2* (Jan 2020), 013044.
- ¹⁵ GEFEN, Y., AHARONY, A., MANDELBRÖT, B. B., AND KIRKPATRICK, S. Solvable fractal family, and its possible relation to the backbone at percolation. *Phys. Rev. Lett.* *47* (Dec 1981), 1771–1774.
- ¹⁶ HALDANE, F. D. M. Model for a Quantum Hall Effect without Landau levels: Condensed-matter realization of the "parity anomaly". *Phys. Rev. Lett.* *61* (Oct 1988), 2015–2018.
- ¹⁷ KEMPKES, S. N., SLOT, M. R., FREENEY, S. E., ZEVENHUIZEN, S. J. M., VANMAEKELBERGH, D., SWART, I., AND SMITH, C. M. Design and characterization of electrons in a fractal geometry. *Nature Physics* *15*, 2 (2019), 127–131.
- ¹⁸ KOLOVSKY, A. R., KORSCH, H. J., AND GRAEFE, E.-M. Bloch oscillations of Bose-Einstein condensates: Quantum counterpart of dynamical instability. *Phys. Rev. A* *80* (Aug 2009), 023617.
- ¹⁹ KRČMAR, R., GENZOR, J., LEE, Y., ČENČARIKOVÁ, H., NISHINO, T., AND GENDIAR, A. Tensor-network study of a quantum phase transition on the Sierpiński fractal. *Phys.*

- Rev. E* 98 (Dec 2018), 062114.
- ²⁰ LIU, C., ZHOU, Y., WANG, G., YIN, Y., LI, C., HUANG, H., GUAN, D., LI, Y., WANG, S., ZHENG, H., LIU, C., HAN, Y., EVANS, J. W., LIU, F., AND JIA, J. Sierpiński Structure and Electronic Topology in Bi Thin Films on InSb(111)B Surfaces. *Phys. Rev. Lett.* 126 (Apr 2021), 176102.
- ²¹ LUCA D'ALESSIO, YARIV KAFRI, A. P., AND RIGOL, M. From quantum chaos and eigenstate thermalization to statistical mechanics and thermodynamics. *Advances in Physics* 65, 3 (2016), 239–362.
- ²² MANDELBROT, B. B. *The fractal geometry of nature*, 3 ed. W. H. Freeman and Comp., New York, 1983.
- ²³ MANNA, S., JAWOROWSKI, B., AND NIELSEN, A. E. B. Many-body localization on finite generation fractal lattices, 2021.
- ²⁴ MANNA, S., NANDY, S., AND ROY, B. Higher-order topological phases on fractal lattices. *Phys. Rev. B* 105 (May 2022), L201301.
- ²⁵ MIELKE, C., DAS, D., YIN, J. X., LIU, H., GUPTA, R., JIANG, Y. X., MEDARDE, M., WU, X., LEI, H. C., CHANG, J., DAI, P., SI, Q., MIAO, H., THOMALE, R., NEUPERT, T., SHI, Y., KHASANOV, R., HASAN, M. Z., LUETKENS, H., AND GUGUCHIA, Z. Time-reversal symmetry-breaking charge order in a Kagome superconductor. *Nature* 602, 7896 (2022), 245–250.
- ²⁶ MIYAKE, H., SIVILOGLOU, G. A., KENNEDY, C. J., BURTON, W. C., AND KETTERLE, W. Realizing the Harper hamiltonian with laser-assisted tunneling in optical lattices. *Phys. Rev. Lett.* 111 (Oct 2013), 185302.
- ²⁷ PAI, S., AND PREM, A. Topological states on fractal lattices. *Phys. Rev. B* 100 (Oct 2019), 155135.
- ²⁸ PAL, B., AND CHAKRABARTI, A. Staggered and extreme localization of electron states in fractal space. *Phys. Rev. B* 85 (Jun 2012), 214203.
- ²⁹ PAL, B., AND SAHA, K. Flat bands in fractal-like geometry. *Phys. Rev. B* 97 (May 2018), 195101.
- ³⁰ PARAOANU, G.-S. Persistent currents in a circular array of Bose-Einstein condensates. *Phys. Rev. A* 67 (Feb 2003), 023607.
- ³¹ POSAZHENNIKOVA, A., TRUJILLO-MARTINEZ, M., AND KROHA, J. Inflationary quasiparticle creation and thermalization dynamics in coupled Bose-Einstein condensates. *Phys. Rev. Lett.* 116 (Jun 2016), 225304.
- ³² POSAZHENNIKOVA, A., TRUJILLO-MARTINEZ, M., AND KROHA, J. Thermalization of isolated Bose-Einstein condensates by dynamical heat bath generation. *Annalen der Physik* 530, 1 (2018), 1700124.
- ³³ RAGHAVAN, S., SMERZI, A., FANTONI, S., AND SHENOY, S. R. Coherent oscillations between two weakly coupled Bose-Einstein condensates: Josephson effects, π oscillations, and macroscopic quantum self-trapping. *Phys. Rev. A* 59 (Jan 1999), 620–633.
- ³⁴ RAMMAL, R. Spectrum of harmonic excitations on fractals. *Journal de Physique* 45, 2 (1984), 191–206.
- ³⁵ RICHTER, K., URBINA, J. D., AND TOMSOVIC, S. Semiclassical roots of universality in many-body quantum chaos. *Journal of Physics A: Mathematical and Theoretical* 55, 45 (Nov 2022), 453001.
- ³⁶ SHANG, J., WANG, Y., CHEN, M., DAI, J., ZHOU, X., KUTTNER, J., HILT, G., SHAO, X., GOTTFRIED, J. M., AND WU, K. Assembling molecular Sierpiński triangle fractals. *Nature Chemistry* 7, 5 (2015), 389–393.
- ³⁷ SMERZI, A., FANTONI, S., GIOVANAZZI, S., AND SHENOY, S. R. Quantum Coherent Atomic Tunneling between Two Trapped Bose-Einstein Condensates. *Phys. Rev. Lett.* 79 (Dec 1997), 4950–4953.
- ³⁸ SREDNICKI, M. Chaos and quantum thermalization. *Phys. Rev. E* 50 (Aug 1994), 888–901.
- ³⁹ TARKHOV, A. E., WIMBERGER, S., AND FINE, B. V. Extracting Lyapunov exponents from the echo dynamics of Bose-Einstein condensates on a lattice. *Phys. Rev. A* 96 (Aug 2017), 023624.
- ⁴⁰ TRUJILLO-MARTINEZ, M., POSAZHENNIKOVA, A., AND KROHA, J. Expansion dynamics in two-dimensional Bose-Hubbard lattices: Bose-Einstein condensate and thermal cloud. *Phys. Rev. A* 103 (Mar 2021), 033311.
- ⁴¹ TSUBOTA, M., AND KASAMATSU, K. Josephson Current Flowing in Cyclically Coupled Bose-Einstein Condensates. *Journal of the Physical Society of Japan* 69, 7 (2000), 1942–1945.
- ⁴² VAN VEEN, E., TOMADIN, A., POLINI, M., KATSNELSON, M. I., AND YUAN, S. Optical conductivity of a quantum electron gas in a Sierpinski carpet. *Phys. Rev. B* 96 (Dec 2017), 235438.
- ⁴³ VAN VEEN, E., YUAN, S., KATSNELSON, M. I., POLINI, M., AND TOMADIN, A. Quantum transport in Sierpinski carpets. *Phys. Rev. B* 93 (Mar 2016), 115428.
- ⁴⁴ VARMA, C. M. Non-Fermi-liquid states and pairing instability of a general model of copper oxide metals. *Phys. Rev. B* 55 (Jun 1997), 14554–14580.
- ⁴⁵ WESTERHOUT, T., VAN VEEN, E., KATSNELSON, M. I., AND YUAN, S. Plasmon confinement in fractal quantum systems. *Phys. Rev. B* 97 (May 2018), 205434.
- ⁴⁶ WOZNIAK, D., KROHA, J., AND POSAZHENNIKOVA, A. Chaos onset in large rings of Bose-Einstein condensates. *Phys. Rev. A* 106 (Sep 2022), 033316.
- ⁴⁷ XU, Y.-L., KONG, X.-M., LIU, Z.-Q., AND YIN, C.-C. Scaling of entanglement during the quantum phase transition for Ising spin systems on triangular and Sierpiński fractal lattices. *Phys. Rev. A* 95 (Apr 2017), 042327.
- ⁴⁸ ZHANG, X., LI, N., LIU, L., GU, G., LI, C., TANG, H., PENG, L., HOU, S., AND WANG, Y. Robust Sierpiński triangle fractals on symmetry-mismatched Ag(100). *Chem. Commun.* 52 (2016), 10578–10581.